Wave Inversion Technology, Report No. 1, pages 97-104

Imaging complex 2D structure with non-Fermat arrival Kirchhoff depth migration

L. Pasasa, F. Wenzel, and P. Zhao[1]

keywords: *not available*

ABSTRACT

Pre-stack Kirchhoff depth migration using Fermat-arrival traveltimes has been shown to produce poor images in areas of complex geologic structure. To avoid this problem, we propose a method for calculating traveltimes that estimates the traveltime of the non-Fermat arrival, rather than the Fermat arrival. To calculate traveltimes of non-Fermat arrivals, we used a method based on Huygens' principle with a curved wavefront assumption. Traveltimes are computed both at grid point and non-grid point of constant slowness cells. At grid points, the incremental traveltimes are computed using Huygens' principle. Then, the arrival time at non-grid points is calculated by a nonlinear interpolation scheme based on a circular wavefront approach. The images created by using these non-Fermat arrivals in a Kirchhoff imaging algorithm are superior to those created using Fermat arrival.

INTRODUCTION

Traveltime computation play an important role in many methods of seismic data processing. For example, Kirchhoff migration requires calculating Green's function, which depend on the traveltimes between survey points on the surface and depth points in the velocity model. Two main approaches for traveltime computation are used in Kirchhoff migration. They are ray tracing methods and the eikonal solution methods.

In the last view years, several methods have been proposed for computing traveltimes in inhomogeneous media on a regular grid to replace the ray tracing method in some applications (e.g. (Vidale, 1988), (Podvin and Lecomte, 1991) and (Schneider et al., 1992)). In this new technique, traveltimes for all grid points are calculated, thus avoiding many of problems associated with ray tracing. However, these finite difference techniques only calculate Fermat arrivals in general. This causes a severe problem when applied to migration in a high velocity contrast media.

In this study, a major modification to Schneider's approach is present, the method is extended to calculate the non-Fermat arrivals.

[1]**email:** lpasasa@gpiwap5.physik.uni-karlsruhe.de

METHOD

The method of traveltime calculation with non-Fermat arrivals generalizes the techniques of (Podvin and Lecomte, 1991). Their technique of a nearest neighbour approximation to Huygens' construction was used to compute Fermat arrival times only. The new technique computes non-Fermat arrival times using the curved wavefront approach of (Schneider et al., 1992), in order to improve the accuracy of the approximation.

When the nearest neighbour approximation to Huygens' principle is used for the traveltime calculation, the time at a grid point is related to the traveltimes at its neighbouring points. Each of these neighbouring points acts as secondary source emitting an impulse. The Fermat arrival time at this point can be obtained by choosing the minimum arrival times from the waves departing from its neighbouring Huygens' sources. However, Huygens' sources are not just limited to the neighbouring grid points. One more approximation is needed. This approximation is to place a Huygens' source on a non grid point. The arrival time at this non grid point is calculated by a nonlinear interpolation scheme.

High velocity boundaries may create head waves and also may produce ”scattered” waves in any direction. These waves can be modeled using reverse propagation toward the source. The reverse mapping uses exactly the same algorithm as the outward mapping. After the outward and reverse propagation, the travel at all target points are computed. At any point (i,j) in a 2D velocity model, the traveltime can be chosen from sixteen potential arrivals (Figure 1). These are the four cell boundary wave arrivals t_{cb} marked (a), the four local diffracted arrivals t_{ld} marked (b), and the eight interpolated arrivals t_{int} marked (c).

The Fermat arrivals t_{Fermat} at the point (i,j) can then be chosen by

$$t_{Fermat} = \min\,(t_{cb}, t_{ld}, t_{int}\,)$$

To compute non-Fermat arrivals, the non-Fermat arrivals $t_{non-Fermat}$ is defined as the minimum between the local diffracted arrival time t_{ld} and the interpolated arrival t_{int} without considering cell boundary arrival waves which are caused by waves traveling along cell boundaries with the faster velocity. Therefore non-Fermat arrival times can be calculated through

$$t_{non-Fermat} = \min\,(t_{ld}, t_{int}\,)$$

SYNTHETIC EXAMPLE

In this section we apply the Kirchhoff migration with Fermat and non-Fermat arrival traveltimes to synthetic data in order to compare them and to demonstrate the versatility and effectiveness of the method.

Traveltime calculation

The subsurface model for the synthetic data consists of a low velocity anomaly of block shape situated in the middle of two layers media. The ratio of the velocities of the anomaly and the background is 1 to 3. The results of traveltime calculations are shown in Figure 2a (Fermat arrival traveltime) and in Figure 2b (non-Fermat arrival traveltime), where constant traveltimes are displayed as contour lines. The circular wavefront generated close to the point source is strongly distorted after passing through the anomaly.

Figure 3 compares the acoustic wavefield modeling with (a) Fermat and (b) non-Fermat arrival times. The figure displays the snapshots times 15, 20, 25 and 30 ms. Fermat times superimposed on the snapshots are located in place with no significant amplitude. In contrast, non-Fermat arrival contours correspond to main portion of the wavefield nicely.

Seismograms

The input seismic data were generated by using the finite-difference acoustic forward modeling program (Sandmeier, 1990). They consist of 9 common-source gathers, where each section contains 48 traces. The direct waves were muted from all synthetic seismograms before performing the migrations. Figure 4 shows a representative common-shot gather with total recording time of 80 ms for a source located at 50 m. The seismograms are complicated. It is not easy to identify the various wave paths and wave types. The first event is a reflection from the top of the low velocity block. The second strong event B represents a reflection from the bottom of the block. The bottom of the block is expected to be reconstructed by migration of this event. Event D are the reflected waves from the second interface at a depth of 80 m. Event A and C are the diffracted waves from both (top and bottom) ends of the block. Between the first and the last events, there are weak event E and F. These weak events are interpreted to be a Fermat traveltime from the lower block and the second interface which propagates back toward the source.

The contour line (Figure 2a) shows the traveltime from S to B to be 22.8 ms and from S to C to be 29 ms. Therefore, the two way traveltime at point S to B is 45.6 ms and from S to C is 58 ms. At 45.6 ms, there is a weak event E on the shot gather shown in Figure 4. It is not the event B which is the reflection from the bottom of the low velocity block. This example shows that the main reflection event from the bottom of the low velocity block can not be the Fermat arrival.

From Figure 2b, the two way traveltime from point S to point B is 54 ms. This is the arrival time of event B which represents the reflections from the bottom block boundary, in the shot gather in Figure 4. From point S to point C, the two way traveltime is 74 ms. This is the traveltime of event D.

Result

Figure 5a shows the result of migration with Fermat arrival times calculated as a finite difference solution of the eikonal equation. While the upper boundary of the block is well imaged, the bottom boundary is totally lost. With Fermat arrival times, the weak event E is mapped to the bottom of the block rather than the main reflected event B. Hence, this method perform well in the simple parts of the velocity model but it fails in the complex regions.

Figure 5b shows the result of migration using non-Fermat arrival times. The image is clearly superior to the Fermat-arrival image. The bottom of the block is properly imaged and the shape of the reflector at 85 m is closer to the truth. Summation along non-Fermat arrival energy trajectories has captured more energy in the reflected wavefield than the Fermat-arrival method.

CONCLUSION

From this example, we conclude that in case the medium contains low velocity areas, non-Fermat arrival traveltime Kirchhoff migration can significantly improve the image when compared to the Fermat-arrival traveltime image.

REFERENCES

REFERENCES

Podvin, P., and Lecomte, I., 1991, Finite-difference computation of traveltimes in very contrasted velocity models: a massively parallel approach and is associated tool: Geophys. J. Int., **105**, 271–284.

Sandmeier, K.-J. Untersuchung der ausbreitungseigenschaften seismischer welle in geschicteten und streunden media:, 1990.

Schneider, W. A. J., Ranzinger, K. A., Balch, A. H., and Kruse, C., 1992, A dynamic programming approach to first arrival traveltime computation in media with arbitrary distributed velocities: Geophysics, **57**, 39–250.

Vidale, J., 1988, Finite-difference calculation of traveltimes: Bull. Seis. Soc., **78**, no. 6, 2062–2076.

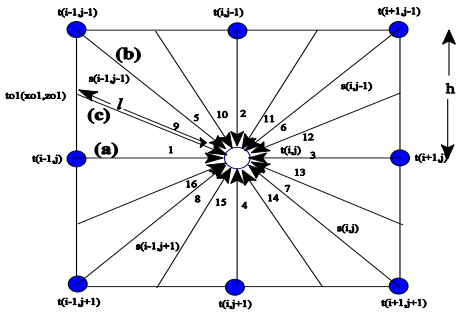

Figure 1: Three types of arrival candidates at point (i,j) from neighbouring cells. They are local cell boundary wave (a), local diffracted wave (b) and interpolated wave (c).

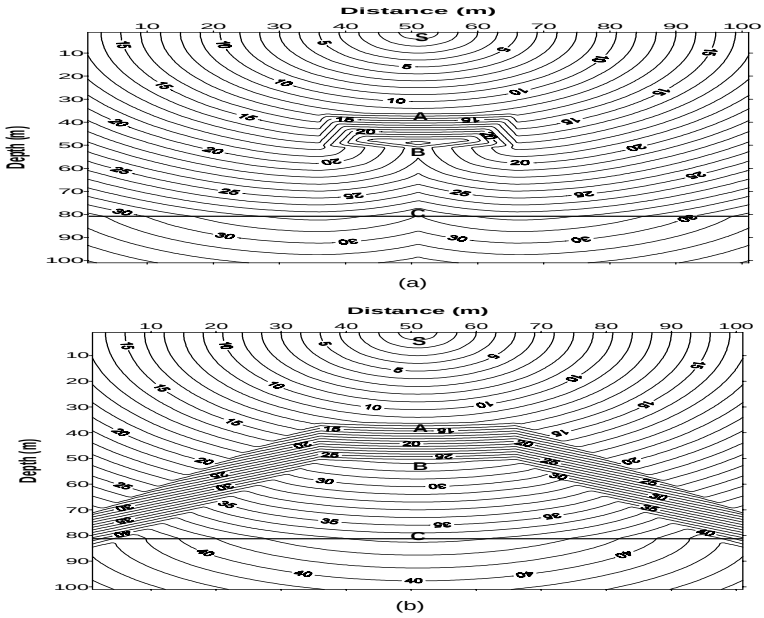

Figure 2: Traveltime maps for the layered model with a low velocity block. The source is of the surface in the center of the model. The traveltime contour lines are drawn at 1 ms intervals. (a) Fermat arrival and (b) non-Fermat arrival maps.

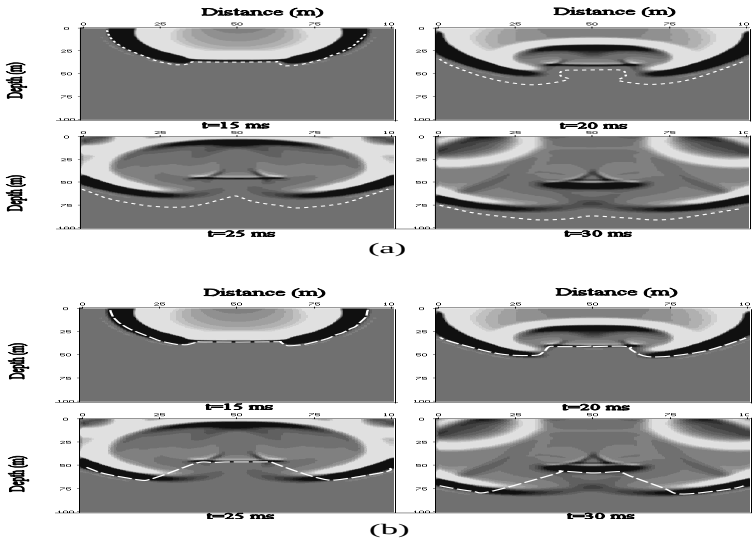

Figure 3: Acoustic wavefield modeling overlaid by Contours of (a) Fermat and (b) non-Fermat traveltimes superimposed on snapshots of the acoustic wavefield at four different times.

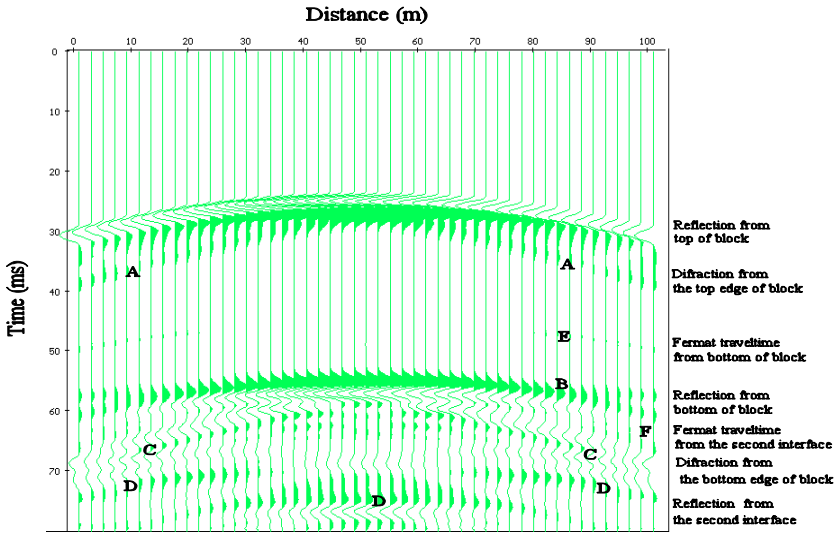

Figure 4: Common shot seismogram of the model calculated by acoustic finite difference modeling, showing a complex wave pattern for times in excess of 40 ms.

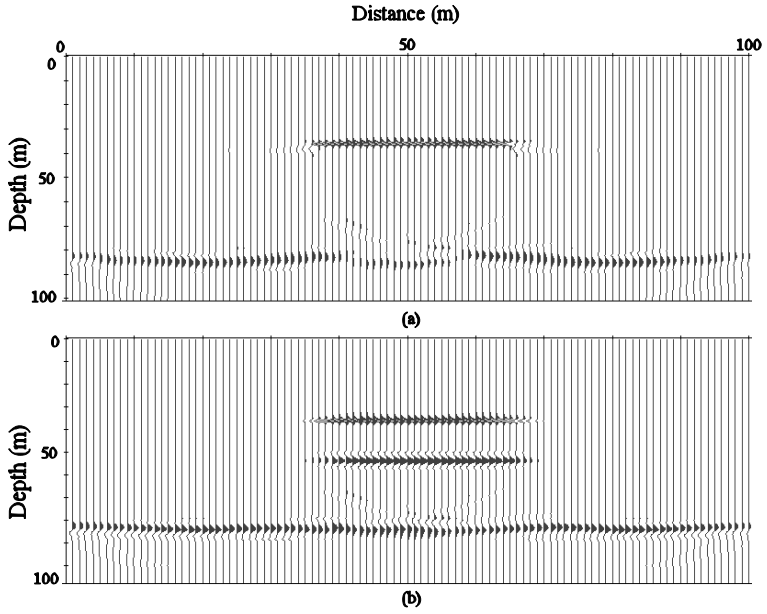

Figure 5: Imaged depth section using nine shots. Image using non-Fermat arrival traveltimes (b) produces superior results as compared to the Fermat arrival image (a). The bottom of the low velocity box is migrated to the correct positions only in case (b).